Received 11 November 2023; accepted 25 November 2023. Date of publication 12 December 2023; date of current version 20 December 2023.

Digital Object Identifier 10.1109/OJCOMS.2023.3339402

Heuristic Antenna Selection and Precoding for a Massive MIMO System

WAQAS BIN ABBAS[1], SALMAN KHALID[2], QASIM ZEESHAN AHMED[3] (Member, IEEE), FARHAN KHALID[2] (Member, IEEE), TEMITOPE T. ALADE[4], AND PRADORN SUREEPHONG[5]

[1]School of Electrical, Electronic and Mechanical Engineering, University of Bristol, BS8 1QU Bristol, U.K.
[2]National University of Computer and Emerging Sciences, Islamabad, Pakistan
[3]Department of Engineering and Technology, University of Huddersfield, HD1 3DH Huddersfield, U.K.
[4]School of Computing Sciences, Faculty of Science, University of East Anglia, NR4 7TJ Norwich, U.K.
[5]College of Arts, Media and Technology, Chiang Mai University, Chiang Mai 50200, Thailand

CORRESPONDING AUTHOR: Q. Z. AHMED (e-mail: q.ahmed@hud.ac.uk)

This work was supported by the European Union through the Horizon Europe Marie Sklodowska-Curie Staff Exchange Programme and EPSRC U.K., "Electric Vehicles Point Location Optimisation via Vehicular Communications (EVOLVE)," under Grant 101086218 and RC Grant EP/X039765/1.

ABSTRACT Sixth Generation (6G) transceivers are envisioned to feature massively large antenna arrays compared to its predecessor. This will result in even higher spectral efficiency (SE) and multiplexing gains. However, immense concerns remain about the energy efficiency (EE) of such transceivers. This work focuses on partially connected hybrid architectures, with the primary aim of enhancing the EE of the system. To achieve this objective, the study proposes a combined approach of joint antenna selection and precoding, which holds the potential to further optimize the system's EE while maintaining a satisfactory SE performance levels. The proposed approach incorporates antenna selection based on a meta-heuristic cyclic binary particle swarm optimization algorithm along with successive interference cancellation-based precoding. The results indicate that the proposed solution, in terms of SE and EE, performs very close to the optimal exhaustive search algorithm. This study also investigates the trade-off between SE and EE in a low and high signal-to-noise ratio (SNR) regimes. The robustness of the proposed scheme is also demonstrated when the channel state information is imperfect. In conclusion, this work presents a lower complexity approach to enhance EE in 6G transceivers while maintaining SE performance and along with a reduction in power consumption.

INDEX TERMS Sixth generation (6G), massive MIMO, antenna selection, hybrid architectures, energy efficiency, power consumption, spectral efficiency, beamforming.

I. INTRODUCTION

OUR PLANET has started witnessing the adverse effects of climate change and immediate efforts from all industry vertical are required to minimize the carbon emission [1], [2]. To reduce the carbon footprint of the information and communication technology (ICT), one of the crucial objectives for future sixth generation (6G) networks is to design them with energy efficiency (EE) as a central criterion [3], [4], [5]. To address this, a hybrid architecture, that comprises of both the analog and digital counter parts, provides a favourable compromise between the spectral efficiency (SE) and EE [6], [7]. Therefore, they have gained considerable attention in the literature [8], [9], [10]. The hybrid architecture is capable of providing beamforming gains using large antenna arrays and multiplexing gain due to the availability of multiple radio frequency (RF) chains.

Numerous techniques for precoding and beamforming have been proposed for both the fully and partially connected architectures [11], [12], [13]. A fully connected hybrid architecture can consume lower energy than a fully digital structure without any significant loss in terms of SE [11], [12], [13]. In [13], the design of a precoder for a

© 2023 The Authors. This work is licensed under a Creative Commons Attribution 4.0 License. For more information, see https://creativecommons.org/licenses/by/4.0/

fully connected architecture is proposed which utilizes the sparsity of the mm-Wave channel and applies the orthogonal matching pursuit (OMP) algorithm. Authors in [14], investigated alternating minimization techniques for the hybrid precoder design. Particularly, phase extraction (PE) and manifold optimization (MO) techniques have been applied to alternatively design the analog and digital precoders. Although MO and OMP algorithms achieve close-to-optimal SE, they have high computational complexity which limits their applicability in a practical scenario.

Due to the power consumption and implementation complexity concerns of a fully connected hybrid architectures, a partially connected hybrid architecture is proposed in [15]. This promising solution represents a step toward lower energy consumption. For such architectures, researchers have explored several precoder design techniques. One approach incorporates a successive interference cancellation (SIC) scheme, resulting in a nearly optimal precoder in terms of EE [15]. Another technique discussed in [16] involves an evolutionary algorithms based scheme known as particle swarm optimization (PSO) algorithm for a precoder design that achieves an EE as close to an optimum precoder. Compared to PSO, a performance improvement using artificial bee colony algorithm is shown in [17]. In another work, signal-to-leakage noise ratio (SLNR) has been used for the design of an analog precoder while the digital precoder is designed with the help of zero forcing (ZF) technique [18].

Although the above algorithms based on the partially connected hybrid architecture have lower energy consumption, the array gain cannot be fully utilized. Consequently, the SE suffers in case of partially connected hybrid architectures. Therefore, a switch-based structure is proposed in [19]. In this context of a hybrid connected architectures, antennas are dynamically allocated to RF chains. A detailed comparison of a fully connected and partially connected architecture is provided in [20]. The precoder design using a SIC-based algorithm is proposed in [21]. Additionally, [22] focuses on designing a precoder based on singular value decomposition (SVD). Therefore, the review of the relevant literature highlights that a fully connected architecture can maximize the SE and a partially connected architecture can provide a more EE solution, while the switched architectures have practical implementation advantages due to higher energy gains.

Higher dimensions of massive multiple-input-multiple-output (MIMO) system can help achieve an improved SE but suffers from an increase in energy consumption [23]. Increasing the number of antennas initially boosts SE, beyond a certain point, the improvement becomes negligible. This limitation has a negative impact on hardware efficiency and power consumption, necessitating careful consideration when expanding the antenna array further [25]. In order to optimize hardware efficiency, authors in [24] have proposed a selection procedure that chooses antennas with favorable channel conditions. The proposed approach is computationally efficient than an optimal exhaustive search (ES) and maintain the advantage of multi-antenna diversity while increasing system efficiency. However, its computational inefficiency necessitates the development of more practical transmit antenna selection schemes capable of managing dynamically changing channel conditions.

Keeping with this view, researchers have explored different approaches for antenna selection, such as minimum eigenvalue techniques and constrained cross-entropy optimization [26]. Euclidean distance based approach for transmit antenna selection was explored in [27]. Furthermore, a comparative analysis of transmit antenna selection systems, considering different receiver architectures, is presented in [28]. In [29], authors proposed genetic algorithm (GA) based antenna selection and showed that the GA perform very close to the optimal exhaustive search based antenna selection. Transmit antenna selection with different types of receivers have been investigated in [30] for full-duplex MIMO systems. In [31], the antenna selection and precoding problem is addressed in a sequential manner. Initially, a subset of antennas are selected using a binary PSO algorithm. Then, SIC based precoding is performed on the reduced channel matrix. Similarly, in [32], antenna selection is performed using evolutionary algorithm while precoding is done utilizing a deep neural network based approach. However, these approaches did not jointly optimize the design of the hybrid beamformer.

Recent research focuses on jointly addressing antenna selection and a hybrid beamformer design. Specifically, [33] investigated the design of an analog precoder employing phase shifters with low-resolution and antenna selection in multiple-input-single-output (MISO) systems. The hybrid beamformer designs and antenna selection proposed in [34] and [35] where quadratic approximation based suboptimal scheme was employed for antenna selection. Authors in [36], focusing on the massive MIMO architecture utilized a greedy search technique to sub-optimally select sub-arrays. In [37], receiver antenna selection for a discrete input in a single input multiple-output (SIMO) system was investigated. Additionally, [38] presented an intelligent antenna selection strategy using a Monte Carlo type search approach to effectively improve system capacity. Furthermore, [39] proposed various transmit antenna selection schemes utilizing matching pursuit techniques to reduce the mean square reception error while minimizing the transmit power consumption and the required number of RF chains. Authors in [40], [41] investigated the antenna selection problem in the presence of low resolution analog-to-digital converters (ADC)s and digital-to-analog converters (DAC)s. Despite employing a range of antenna selection criteria and optimization strategies, the work on the joint antenna selection and precoding is still limited. In this paper, our focus is on improving the EE of a partially connected hybrid architecture equipped with massively large antenna arrays by devising an efficient

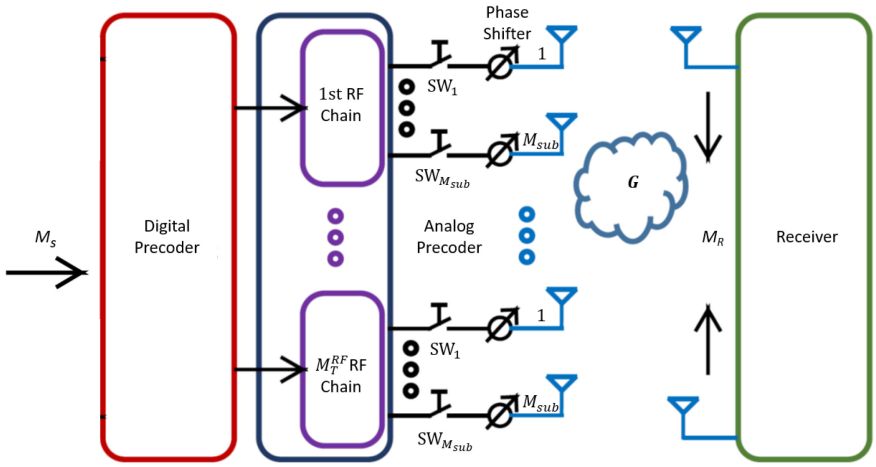

FIGURE 1. Block diagram of the considered partially connected architecture with antenna selection.

scheme for simultaneous antenna selection and precoding. Particularly, the key contributions of this work are:

- To address the challenge of simultaneous antenna selection and precoding, a hybrid heuristic approach is presented. A metaheuristic cyclic binary particle swarm optimization (cBPSO) algorithm for selecting a subset of antennas and a SIC based algorithm for hybrid precoding is proposed.
- The proposed scheme performs very close to the optimal ES based scheme, despite having lower complexity. It outperforms both the GA and the SIC based joint antenna selection and precoding, as well as a BPSO plus SIC scheme.
- The proposed scheme demonstrates the ability to enhance the EE without experiencing any notable performance loss in terms of SE. The study reveals the presence of an optimal number of antennas that maximizes the EE, providing valuable insights for efficient antenna configuration.
- The proposed scheme can be extended to a wideband system, and a negligible difference in performance is observed when compared to a narrowband system.
- The proposed scheme is computationally efficient, achieving lower complexity when compared to state-of-the-art methods.
- The robustness of the proposed scheme is demonstrated in scenarios where channel state information is not perfect.

The subsequent sections of this manuscript are structured as follows: Section II elucidates the considered system model. Section III starts with the antenna selection problem formulation and then discusses in detail the antenna selection and precoding algorithms in Sections III-A and III-B, respectively. Section IV is dedicated to presenting simulation results, wherein the performance of the proposed scheme is evaluated. Finally, Section V provides the conclusions.

In this manuscript, matrices and vectors are represented by a boldface uppercase **B** and a lower case **b** letters, respectively. $|.|$ and $(.)^{-1}$ refer to the determinant and matrix inverse, whereas $(.)^H$ and $(.)^T$ correspond to conjugate transpose and transpose, respectively. $\mathbf{I}_M$ represents an $M \times M$ identity matrix. Finally, Frobenius norm is donated by $\|\cdot\|_{\mathcal{F}}$.

II. SYSTEM MODEL

This work investigates a MIMO communication system. The transmitter is equipped with massively large number of antennas M_T while the receiver is has M_R antennas as shown in Figure 1. To support multi-stream communication, the transmitter has M_T^{RF} radio frequency chains, where $M_T^{RF} < M_T$. There are total M_T^{RF} sub-arrays and it is considered that each RF chain is connected to a sub-array containing a subset of antennas M_{sub}, i.e., $M_{sub} = M_T/M_T^{RF}$. The system can support communication of M_S data streams, and it is considered that $M_S \leq M_T^{RF}$. The receiver in this study is assumed to be fully digital, implying that the number of RF chains at the receiver is equal to M_R. Furthermore, M_T^{Sel} corresponds to the number of selected antennas in each sub-array and M_{Sel} represents the total number of selected antennas at the transmitter. Now considering a fully operational antenna array at the transmitter, the received signal with hybrid precoding at the transmitter can be expressed as

$$\mathbf{r} = \sqrt{p}\mathbf{G}\mathbf{\Psi}\mathbf{s} + \mathbf{v}, \tag{1}$$

where p is the average received power, $\mathbf{r} \in \mathbb{C}^{M_R \times 1}$ represents the received signal vector and $\mathbf{v}$ is the independent and identically distributed circularly symmetric complex Gaussian noise having $\mathcal{CN}(0, \sigma^2)$. $\mathbf{s}$ represents the transmitted symbol vector with $\mathbb{E}\{\mathbf{s}\mathbf{s}^H\} = \frac{1}{M_S}\mathbf{I}_{M_S}$. $\mathbf{\Psi}$ is the transmitter precoding matrix comprising of both the analog and digital precoders. A further discussion on the hybrid precoder formulation will be provided later. Finally, $\mathbf{G}$ represents the channel matrix of dimensionality $\mathbf{G} \in \mathbb{C}^{M_R \times M_T}$ with a perfectly known channel state information.

This work is focused on the narrowband wireless communication channel and adopted the Saleh-Valenzula model

to capture the characteristics of the MIMO channel. It is considered that the transmitter and receiver are equipped with a uniform linear array (ULA). With that the channel matrix $\mathbf{G}$ is given as

$$\mathbf{G} = \rho \sum_{k=0}^{K} \xi_k \boldsymbol{\eta}_R(\alpha_k) \boldsymbol{\eta}_T^H(\beta_k), \tag{2}$$

where K represents the total number of paths and ρ is given as

$$\rho = \sqrt{(M_T M_R)/K}, \tag{3}$$

ξ_k is the complex gain corresponding to the kth path. $\boldsymbol{\eta}_R(\alpha_k)$ and $\boldsymbol{\eta}_T(\beta_k)$ represent the spatial signatures corresponding to the receiver and transmitter, respectively, and considering a ULA they are given as

$$\boldsymbol{\eta}_R(\alpha) = \frac{1}{\sqrt{M_R}}\left[1, \exp^{j\kappa \sin\alpha}, \ldots, \exp^{j(M_R-1)\kappa \sin\alpha}\right]^T, \tag{4}$$

$$\boldsymbol{\eta}_T(\beta) = \frac{1}{\sqrt{M_T}}\left[1, \exp^{j\kappa \sin\beta}, \ldots, \exp^{j(M_T-1)\kappa \sin\beta}\right]^T, \tag{5}$$

where $\kappa = \frac{2\pi d}{\lambda}$ with d representing the spacing between the antenna elements, and α and β represent the angle of arrival and departure, respectively.

The hybrid precoding matrix $\boldsymbol{\Psi}$ can be separated into an analog precoder $\boldsymbol{\Psi}_{RF}$ and a lower dimensional digital precoder $\boldsymbol{\Psi}_{BB}$, such that $\boldsymbol{\Psi} = \boldsymbol{\Psi}_{BB}\boldsymbol{\Psi}_{RF}$, and satisfying that the power constraint is normalized, $||\boldsymbol{\Psi}_{BB}\boldsymbol{\Psi}_{RF}||_F^2 = M_S$. Furthermore, the RF precoder should also satisfy the equal norm constraint for each element $[[F_{RF}]_{:,i}[F_{RF}]_{:,i}^H]_{i,i} = 1/M_T$. For a partially connected hybrid, the analog beamforming matrix $\boldsymbol{\Psi}_{RF} \in \mathbb{C}^{M_T \times M_T^{RF}}$ exhibits a block diagonal structure and can be given as

$$\boldsymbol{\Psi}_{RF} = \begin{bmatrix} \boldsymbol{\psi}_{RF_1} & \mathbf{0} & \cdots & \mathbf{0} \\ \mathbf{0} & \boldsymbol{\psi}_{RF_2} & \cdots & \mathbf{0} \\ \vdots & \vdots & \ddots & \vdots \\ \mathbf{0} & \mathbf{0} & \cdots & \boldsymbol{\psi}_{RF_{M_T^{RF}}} \end{bmatrix}, \tag{6}$$

where $\boldsymbol{\psi}_{RF_i}$ represents the analog precoding vector corresponding to the ith sub-array connected to ith RF chain. To reduce the complexity of the design the digital precoding matrix $\boldsymbol{\Psi}_{BB} \in \mathbb{C}^{M_T^{RF} \times M_T^{RF}}$ can be expressed as a diagonal matrix [15], [42]. In such a case, the digital precoder is essentially allocating power to different RF streams and is given as

$$\boldsymbol{\Psi}_{BB} = \begin{bmatrix} \psi_{BB_1} & 0 & \cdots & 0 \\ 0 & \psi_{BB_2} & \cdots & 0 \\ \vdots & \vdots & \ddots & \vdots \\ 0 & 0 & \cdots & \psi_{BB_{M_T^{RF}}} \end{bmatrix}. \tag{7}$$

Considering the transmission of Gaussian symbols the SE can be expressed as

$$\Gamma(\boldsymbol{\Psi}) = \log_2\left(\left|\mathbf{I}_{M_R} + \frac{p}{M_T^{RF}\sigma^2}\mathbf{G}\boldsymbol{\Psi}\boldsymbol{\Psi}^H\mathbf{G}^H\right|\right), \tag{8}$$

$$\Gamma(\boldsymbol{\Psi}_{BB}, \boldsymbol{\Psi}_{RF}) = \log_2\left(\left|\mathbf{I}_{M_R} + \frac{p}{M_T^{RF}\sigma^2} \times \mathbf{G}\boldsymbol{\Psi}_{BB}\boldsymbol{\Psi}_{RF}\boldsymbol{\Psi}_{RF}^H\boldsymbol{\Psi}_{BB}^H\mathbf{G}^H\right|\right). \tag{9}$$

Let us now present the formulation of a joint antenna selection and precoding problem followed by a detailed discussion on the proposed cBPSO algorithm for an antenna selection and SIC algorithm for precoding.

III. JOINT ANTENNA SELECTION AND PRECODING

The goal is to simultaneously identify the subset of antennas and design a hybrid precoder that result in a maximization of SE. An iterative process is adopted as it is dependant on the availability of the channel matrix $\mathbf{G}$. The first step is to efficiently pick M_{Sel} from M_T antennas. This will result in a reduced size channel matrix given as, $\tilde{\mathbf{G}} = \mathbf{GS}$ of size $M_R \times M_{Sel}$. Here, $\mathbf{S}$ represents the $M_T \times M_{Sel}$ selection matrix where a particular $[\mathbf{S}]_{i,j}$ entry can be either 0 or 1. In the next step, using the reduced channel matrix $\tilde{\mathbf{G}}$, the aim is to design a precoder that will maximize the SE of the system. It is required to repeat these steps until a near-optimal subset of antennas is selected such that further iteration would not result in any notable increase in SE. Particularly, the design of the simultaneous antenna selection and hybrid precoder design should satisfy

$$\begin{aligned} (\tilde{\boldsymbol{\Psi}}_{BB}^{opt}, \tilde{\boldsymbol{\Psi}}_{RF}^{opt}, \mathbf{S}) = \underset{\tilde{\boldsymbol{\Psi}}_{BB}, \tilde{\boldsymbol{\Psi}}_{RF}, \mathbf{S}}{\arg\max} \ & \log_2\left(\left|\mathbf{I}_{M_R} \right.\right. \\ & \left.\left. + \frac{p}{M_T^{RF}\sigma^2}\tilde{\mathbf{G}}\tilde{\boldsymbol{\Psi}}_{BB}\tilde{\boldsymbol{\Psi}}_{RF}\tilde{\boldsymbol{\Psi}}_{RF}^H\tilde{\boldsymbol{\Psi}}_{BB}^H\tilde{\mathbf{G}}^H\right|\right) \\ \text{subject to} : \ & \tilde{\boldsymbol{\Psi}}_{RF} \in \mathcal{P}_{RF}, \\ & ||\tilde{\boldsymbol{\Psi}}_{RF}\tilde{\Psi}_{BB}||_{\mathcal{F}}^2 = M_S, \\ & ||\text{diag}\{\mathbf{S}\}||_0 = M_{Sel}, \end{aligned} \tag{10}$$

here $\tilde{\boldsymbol{\Psi}}_{RF}$ is the analog precoder corresponding to a reduced channel matrix $\tilde{\mathbf{G}}$. M_{Sel} is the number of selected antennas. Finally, $\mathcal{P}_{RF}$ represents the set of feasible analog beamformer. To solve the above problem, $\mathbf{S}$ is computed using cBPSO whereas the optimal precoding matrices are evaluated using SIC algorithm.

Finally, EE of the system is quantified as

$$\text{EE} = \frac{\Gamma(\boldsymbol{\Psi})}{P_{Tot}} \quad \text{(bps/Hz/Watts)}, \tag{11}$$

where P_{Tot} represents the total power consumption. Note that P_{Tot} is independent of the combination of selected antennas whereas SE varies with that. Therefore, a maximization of SE implicitly identifies the best subset of selected antennas and that also maximizes the EE.

A. ANTENNA SELECTION

Future transceivers are envisioned to be equipped with extremely large antenna arrays that intensify the power/energy consumption concerns. Antenna selection is a viable solution to tackle this problem. Nevertheless,

choosing the most suitable subset of antennas from an extremely large antenna array could lead to a considerable increase in computational complexity. For instance, ES can generate an optimal solution (at the cost of a very high computational complexity) by exploiting the complete search space, i.e., $\mathcal{S}_c = \binom{M_{Sub}}{M_T^{Sel}}$, where M_T^{Sel} represents the selected antennas at any particular sub-array. Let $\mathcal{W}$ represents the set containing all the combination of the selected antennas, $\mathcal{W} = \{\mathcal{W}_1, \mathcal{W}_2, \ldots, \mathcal{W}_{\mathcal{S}_c}\}$, where subset $\mathcal{W}_j$ corresponds to the jth combination of the selected antennas out of $\mathcal{S}_c$ combinations. By extending the same formulation for M_T^{RF} sub-arrays, the total number of combinations will be $\mathcal{S}_t = (\mathcal{S}_c)^{M_T^{RF}}$. Let $\mathcal{X}$ corresponds to the set (search space) that contains all the combinations of selected antennas for M_T^{RF} sub-arrays, i.e., $\mathcal{X} = \{\mathcal{X}_1, \mathcal{X}_2, \ldots, \mathcal{X}_{\mathcal{S}_t}\}$, and the kth entry of $\mathcal{X}$ corresponds to the kth combination of the selected antennas. Furthermore, $\mathcal{X}_k$ is a vector of size M_T, with entries either equal to '0' or '1', where '1' corresponds to the selected antenna. Given the kth configuration of the selected antennas $\mathcal{X}_k$ the received signal is given as

$$\mathbf{r}_{\mathcal{X}_k} = \sqrt{p}\tilde{\mathbf{G}}_{\mathcal{X}_k}\tilde{\mathbf{\Psi}}_{\mathcal{X}_k}\mathbf{s} + \mathbf{v}, \tag{12}$$

where $\tilde{\mathbf{G}}_{\mathcal{X}_k} = \mathbf{G}\mathbf{S}_{\mathcal{X}_k}$ represents the reduced size channel matrix corresponding to the $\mathcal{X}_k$ selected antennas combination, and $\tilde{\mathbf{\Psi}}_{\mathcal{X}_k}$ represents the corresponding precoding matrix. Finally, the corresponding SE is given as

$$\Gamma\left(\mathbf{\Psi}_{\mathcal{X}_k}\right) = \log_2\left(\left|\mathbf{I}_{M_R} + \frac{p}{M_T^{RF}\sigma^2}\tilde{\mathbf{G}}_{\mathcal{X}_k}\tilde{\mathbf{\Psi}}_{\mathcal{X}_k}\tilde{\mathbf{\Psi}}_{\mathcal{X}_k}^H\tilde{\mathbf{G}}_{\mathcal{X}_k}^H\right|\right). \tag{13}$$

Note that the SE is dependent on $\mathcal{X}_k$ through $\tilde{\mathbf{G}}_{\mathcal{X}_k}$. The aim is to select the best subset of antennas from all the available combinations that maximizes the SE, i.e.,

$$\hat{\mathcal{X}}_k = \underset{\mathcal{X}_k \in \mathcal{X}}{\arg\max} \quad \Gamma\left(\tilde{\mathbf{\Psi}}_{\mathcal{X}_k}\right), \tag{14}$$

where $\hat{\mathcal{X}}_k$ corresponds to the combination of selected antennas that maximizes the SE.

ES algorithm can provide an optimal solution but the computational complexity grows exponentially with an increase in the number of antennas [43]. This technique is not appropriate for actual implementation since it would be computationally costly to evaluate every combination. In contrast to the ES, the random search algorithm chooses a subset of antennas for processing at random. This typically leads to a decrease in the SE due to the random nature of the scheme. Therefore, the goal is to develop a computationally efficient antenna selection solution without any significant performance loss compared to an ES based solution. To address this, a meta heuristic algorithm, i.e., cBPSO is proposed for the antenna selection. Considering the availability of the channel state information, the idea is to explore the channel matrix $\mathbf{G}$ of the full dimensional antenna array and then picks a subset of antennas, that correspond to a reduced channel matrix $\tilde{\mathbf{G}}$, that will result in power savings but without any significant loss in the SE of the system. The next part will first provide the details of the BPSO algorithm. Then the idea will be extended to a cBPSO scheme.

1) BPSO FOR ANTENNA SELECTION

BPSO is a binary variant of PSO, which is a population based collaborative meta-heuristic scheme inspired by the birds flock behavior. Every individual bird may be referred to as an independent agent in PSO, and a population is a group of agents (or swarm) [43]. If we formulate the optimization problem as a maximization problem of $\Gamma(\mathbf{\Psi}_{\mathcal{X}_k})$ corresponding to the position vectors (x_1, x_2, x_3, …, x_{M_T}) of agents, where $x_j \in (0, 1)$ illustrates whether the jth antenna from the available M_T antennas is selected or not. Note that the M_T dimensional position vector of each agent corresponds to one of the entry in set $\mathcal{X}$. Exploring the search space (in context of this work, it is represented as $\mathcal{X}$) to evaluate the best solution is analogous to agents flying in the search space to discover the optimal position, i.e., the best subset from set $\mathcal{X}$. In PSO, agents update their position with respect to time (iteration in the context of this work) i.e., agents fly around (to update their position) in an M_T-dimensional search space. Every agent updates its position based on the self experience and neighbouring agent experience. Hence, the local search is also combined with the global search to evaluate a better solution.

In this work, the antenna selection problem is formulated as a binarized optimization problem and BPSO algorithm is applied to identify the optimal subset $\hat{\mathcal{X}}_k$. In BPSO, the location of an agent is represented as a string of binary digits (bits) consisting of '0' and '1', where in context of the considered setup '1' and '0' correspond to a selected and non-selected antenna, respectively. Note that the search space of a PSO algorithm is continuous, however the output is mapped to a discrete search space as required in BPSO. This is achieved with a help of a transfer function, which is an important part of the BPSO scheme. In this work, an S shaped function, $S(z) = (1 + \exp(-z))^{-1}$ is utilized to map a continuous signal to a binarized search space [44]. By manipulating bits, each agent can migrate from its current place (a vector $\mathcal{X}_k$ with entries corresponding to a selected and non-selected antennas) to any other viable point (a vector $\mathcal{X}_k^{\text{up}}$ that correspond to an updated entries corresponding to a selected and non-selected antennas), i.e., in the search space $\mathcal{X}$.

Generally, BPSO is characterized by the following parameters and notations.

- $\mathcal{X}$*:* Solution Space of all possible candidates. In current paper scenario, $\mathcal{X}$ is the set of all possible scenarios of antenna selection vectors.
- Fitness function against the different agents is evaluated. In this paper, fitness function corresponds to $\Gamma(\mathbf{\Psi}_{\mathcal{X}_k})$, i.e., the achieved SE to a corresponding agent $\mathcal{X}_k$ and is computed using equation Eq. (13). The agent which will maximize the SE will be chosen.

- M_{pop}: Size of the population (or number of agents). It is the basic parameter of the BPSO algorithm. M_{pop} is selected keeping in view the computational complexity. A higher value of M_{pop} corresponds to a higher computational complexity.
- M_{Iter}: Maximum number of iterations. It is the basic BPSO parameters. M_{iter} is selected keeping in view the computational complexity.
- D_{AP}: Refers to the length (or dimension) of the binary string representing the position of the agent. In this work, dimension of the agent is equivalent to M_T.
- Ω^i: Collection of position of agents at the ith iteration, represented as $\Omega^i = [\mathbf{x}_1^i, \mathbf{x}_2^i, \ldots, \mathbf{x}_{M_T}^i]$. Here $\mathbf{x}_l^i = [x_{1,l}^i, x_{2,l}^i, \ldots, x_{M_T,l}^i]^T$ represents the position of the lth agent at the ith iteration, where $\mathbf{x}_{k,l}^i \in (0, 1), k = 1, 2, \ldots, M_T$. In this paper, $\mathbf{x}_l^i$ is the antenna selection vector corresponding to an entry in the set $\mathcal{X}$.
- $\mathbf{p}_{best}$: Personal best position vector of each agent experienced by any agent during BPSO operation.
- ∇_{best}: Global best position vector that resulted in a maximum SE. It is the best among the personal best position vectors experienced by every agent.

2) EXTENSION TO CBPSO

In this section, we present the modification in BPSO. Note that the traditional BPSO algorithm generates the initial population randomly. The random initialization of a population may raise an issue as a particular antenna (or set of antennas) may remain deactivated through out the selection procedure. Thereby, resulting in selecting a sub-optimal antenna subset. To address this issue, cyclic shift property is adopted making sure that each antenna is selected at least once. This fundamental approach revolves around generating the initial string randomly and then utilizing cyclic shifts to determine the initial positions of the agents. This guarantees an unbiased initial selection of antennas, resulting in an equal opportunity for all antennas to be selected. Therefore the use of cyclic shifts resolves the issue associated with the random initialization and thus help us in improving SE. Finally, the proposed cBPSO algorithm is summarised as Algorithm 1.

Algorithm 1 cBPSO Algorithm for Transmit Antenna Selection

Initialize: M_{pop}, M_{Iter}, M_{Sel}

(Step 1) Generate the initial positions x and velocities z corresponding to the population using the cyclic shifts on the initial feed. At the first iteration (i = 0), set $\mathbf{p}_{best,1}^0 = \mathbf{x}_1^0$, $\mathbf{p}_{best,2}^0 = \mathbf{x}_2^0$, $\ldots$, $\mathbf{p}_{best,M_{pop}}^0 = \mathbf{x}_N^0$. Similarly, $\nabla_{best}^0 = \underset{1<k<M_{pop}}{\arg\max}\ \Gamma(\tilde{\mathbf{\Psi}}_{\mathbf{x}_k^0})$.

(Step 2) Update the velocity for each agent as

$$\mathbf{z}_k^i = \mathbf{z}_k^{i-1} + d_1 \times \mathcal{U}(0,1) \times \left(\nabla_{best}^{i-1} - \mathbf{x}_k^{i-1}\right) + d_2 \times \mathcal{U}(0,1) \times \left(\mathbf{p}_{best_k}^{i-1} - \mathbf{x}_k^{i-1}\right), \quad (15)$$

where d_1 and d_2 corresponds to the social and cognitive parameters and are used to change in movement of the agents.

(Step 3) Update position of all agents using

$$[x_k^i]_j = \begin{cases} 1, & \text{if } \mathcal{U}(0,1) \le \sigma([\mathbf{z}_k^i]_j) \\ 0, & \text{Otherwise.} \end{cases}$$

(Step 4) if $(||\mathbf{x}_k^i||_0 \neq M_{Sel}) \rightarrow$ Repair the result by randomly inverting values to ensure $||\mathbf{x}_k^i||_0 = M_{Sel}$. The BPSO algorithm output the indices of selected antennas, however, it may not be a subset of $\mathcal{X}$. Hence, the bits are randomly inverted for each sub-array so that the resultant sub-array is a subset of $\mathcal{W}$.

(Step 5) For each agent, obtain the corresponding reduced channel matrix $\tilde{\mathbf{G}}$.

(Step 6) Apply SIC algorithm on the reduced channel matrix $\tilde{\mathbf{G}}_{\mathbf{x}_k^i}$ to obtain the precoding matrix $\tilde{\mathbf{\Psi}}_{\mathbf{x}_k^i}$.

(Step 7) Evaluate the fitness function $\Gamma(\tilde{\mathbf{\Psi}}_{\mathbf{x}_k^i})$ according to the position of agents and set $\mathbf{p}_{best,k}^{up} = \mathbf{x}_k^i$.

(Step 8) Update $\mathbf{p}_{best}$ of each agent ($k = 1, 2, ..., M_{pop}$).
if $\Gamma(\tilde{\mathbf{\Psi}}_{\mathbf{p}_{best,k}^{up}}) > \Gamma(\tilde{\mathbf{\Psi}}_{\mathbf{p}_{best,k}^{i-1}})$,
$\mathbf{p}_{best,k}^i = \mathbf{p}_{best,k}^{up}$,
else
$\mathbf{p}_{best,k}^i = \mathbf{p}_{best,k}^{i-1}$

(Step 9) Update the global best position
$\nabla_{best}^i = \underset{1<k<M_{pop}}{\arg\max}\ \Gamma(\tilde{\mathbf{\Psi}}_{\mathbf{p}_{best,k}^i})$.

(Step 10) Check the termination rule. If it does not meet, go to step 2 and repeat.

B. HYBRID PRECODER DESIGN

A reduced channel matrix $\tilde{\mathbf{G}}$ is generated in step 5 of the Algorithm 1. Then this low dimensional matrix is used to find the best precoder using the SIC algorithm. Then using that precoder, SE is evaluated. After that based on the criteria mentioned in Algorithm 1, positions of the particles are updated for the next iteration.

This work is mainly focused on the hybrid precoder design, since the joint optimization of the precoder and the combiner is found to be intractable due to non-convex constraints on phase shifters [13]. Focusing on the hybrid precoder design, the optimization problem is given as

$$\begin{aligned}(\tilde{\mathbf{\Psi}}_{BB}^{opt}, \tilde{\mathbf{\Psi}}_{RF}^{opt}) &= \underset{\tilde{\mathbf{\Psi}}_{BB}, \tilde{\mathbf{\Psi}}_{RF}}{\arg\max} \quad \Gamma\left(\tilde{\mathbf{\Psi}}_{BB}, \tilde{\mathbf{\Psi}}_{RF}\right), \\ &= \underset{\tilde{\mathbf{\Psi}}_{BB}, \tilde{\mathbf{\Psi}}_{RF}}{\arg\max} \quad \Gamma\left(\tilde{\mathbf{\Psi}}\right), \end{aligned} \quad (16)$$

where $\tilde{\mathbf{\Psi}}$ and $\tilde{\mathbf{\Psi}}_{RF}$ are the overall and analog precoding matrices, respectively, corresponding to the channel matrix obtained after antenna selection. Note that the there will be no effect on the dimensions of the digital precoding matrix

due to the antenna selection. Considering the structure of $\tilde{\boldsymbol{\Psi}}$, there are three constraints on the precoding matrices design:

Constriant 1: The precoding matrix $\tilde{\boldsymbol{\Psi}}$ should be a block diagonal matrix with a similar structure as of $\tilde{\boldsymbol{\Psi}}_{RF}$, i.e., $\tilde{\boldsymbol{\Psi}} = \text{diag}\{\tilde{\boldsymbol{\psi}}_1, \tilde{\boldsymbol{\psi}}_2, \ldots, \tilde{\boldsymbol{\psi}}_{M_T^{RF}}\}$, with $\tilde{\boldsymbol{\psi}}_i = \psi_{BB_i}\tilde{\boldsymbol{\psi}}_{RF_i}$ is the non-zero vector of size M_T^{Sel} in the ith column of $\tilde{\boldsymbol{\Psi}}$.

Constraint 2: To ensure the total power constraint, the Frobenius norm of $\tilde{\boldsymbol{\Psi}}$ needs to satisfy that $||\tilde{\boldsymbol{\Psi}}||_F \leq M_T^{RF}$.

Constraint 3: The digital precoder $\boldsymbol{\Psi}_{BB}$ represents a diagonal matrix whereas the amplitude of the non-zero elements of analog precoder $\tilde{\boldsymbol{\Psi}}_{RF}$ are set to $1/\sqrt{M_{sub}}$. Thus, the non-zero elements in each column of the precoding matrix $\tilde{\boldsymbol{\Psi}}$ should have the same amplitude.

The achievable rate optimization problem is very difficult to solve due the non-convex constraints on the precoder matrix $\tilde{\boldsymbol{\Psi}}$. Despite that the diagonal structure of the antenna arrays allows to perform precoding on different sub-arrays of antennas independently. This leads to decomposing the optimization problem in (16) to a series of sub SE maximization problems [15]. Note that the each sub-problem corresponds to a sub-array of antennas.

Based on that the hybrid precoding matrix can be divided as $\tilde{\boldsymbol{\Psi}} = [\tilde{\boldsymbol{\Psi}}_{M_T^{RF}-1}\ \tilde{\boldsymbol{\psi}}_{M_T^{RF}}]$, where matrix $\tilde{\boldsymbol{\Psi}}_{M_T^{RF}-1}$ has a size $M_T^{RF}M_T^{Sel} \times (M_T^{RF}-1)$ and contains the first $(M_T^{RF}-1)$ columns of $\tilde{\boldsymbol{\Psi}}$, and $\tilde{\boldsymbol{\psi}}_{M_T^{RF}}$ is the M_T^{RF}th column of $\tilde{\boldsymbol{\Psi}}$. Accordingly, the SE is given as

$$\Gamma\left(\tilde{\boldsymbol{\Psi}}\right) = \log_2\left(\left|\mathbf{P}_{M_T^{RF}-1}\right|\right) + \log_2\left(\left|\mathbf{I}_{M_R} + \frac{p}{M_T^{RF}\sigma^2}\tilde{\boldsymbol{\psi}}_{M_T^{RF}}^H\tilde{\mathbf{G}}^H\mathbf{P}_{M_T^{RF}-1}^{-1}\tilde{\mathbf{G}}\tilde{\boldsymbol{\psi}}_{M_T^{RF}}\right|\right), \tag{17}$$

where $\mathbf{P}_{M_T^{RF}-1} = \mathbf{I}_{M_R} + \frac{p}{M_T^{RF}\sigma^2}\tilde{\mathbf{G}}\mathbf{P}_{M_T^{RF}-1}\mathbf{P}_{M_T^{RF}-1}^H\tilde{\mathbf{G}}^H$. It is highlighted that the second term, i.e., $\log_2(|\mathbf{I}_{M_R} + \frac{p}{M_T^{RF}\sigma^2}\tilde{\boldsymbol{\psi}}_{M_T^{RF}}\tilde{\mathbf{G}}\mathbf{P}_{M_T^{RF}-1}\tilde{\mathbf{G}}^H\tilde{\boldsymbol{\psi}}_{M_T^{RF}}^H|)$ of (17) corresponds to the rate of M_T^{RF}th antenna sub-array. Using the same approach, $\mathbf{P}_{M_T^{RF}-1}$ can be further decomposed. Hence, after $M_T^{RF}-1$ decompositions, the overall SE can be expressed as

$$\Gamma\left(\tilde{\boldsymbol{\Psi}}\right) = \sum_{m=1}^{M_T^{RF}}\log_2\left(\left|\mathbf{I}_{M_R} + \frac{p}{M_T^{RF}\sigma^2}\tilde{\boldsymbol{\psi}}_m^H\tilde{\mathbf{G}}^H\mathbf{P}_{m-1}^{-1}\tilde{\mathbf{G}}\tilde{\boldsymbol{\psi}}\right|\right), \tag{18}$$

where $\mathbf{P}_m = \mathbf{I}_{M_R} + \frac{p}{M_T^{RF}\sigma^2}\tilde{\mathbf{G}}\mathbf{P}_m\mathbf{P}_m^H\tilde{\mathbf{G}}^H$, and for consistency $\mathbf{P} = \mathbf{I}_N$, in the case of $M_T^{RF} = 0$. Note that based on (18), the SE maximization problem can now be solved sequentially by addressing the optimization of each sub-array one by one. Based on this formulation, this papers utilizes the SIC algorithm to optimize the SE. It starts by optimizing the sub-rate of the first antenna sub-array and updating the corresponding matrix $\mathbf{P}_1$. This process can be continued until the last antenna sub-array is considered.

Next step is to find the mth precoder corresponding to the mth sub-array. Let $\mathbf{Q} = \tilde{\mathbf{G}}^H\mathbf{P}_{m-1}^{-1}\tilde{\mathbf{G}}$ and Υ representing the set of feasible vectors fulfilling the precoder design constraints. With that the optimization problem can be formulated as

$$\tilde{\boldsymbol{\psi}}_m^{opt} = \arg\max_{\tilde{\boldsymbol{\psi}}_m \in \Upsilon}\ \sum_{m=1}^{M_T^{RF}}\log_2\left(\left|\mathbf{I}_{M_R} + \frac{p}{M_T^{RF}\sigma^2}\tilde{\boldsymbol{\psi}}_m^H\mathbf{Q}_{m-1}\tilde{\boldsymbol{\psi}}_m\right|\right), \tag{19}$$

It can be observed that the precoding vector $\tilde{\boldsymbol{\psi}}_m$ has M_{Sub} non-zero elements. With that consider a modified matrix $\breve{\mathbf{Q}}_{m-1}$ that keeps the $(M_{Sub}(m-1)+1)$ till $(M_{Sub}m)$ rows and columns of $\mathbf{Q}_{m-1}$ and let $\breve{\Upsilon}$ is a vector of size M_{Sub}, the equivalent form of (19) is given as

$$\tilde{\boldsymbol{\psi}}_m^{opt} = \arg\max_{\tilde{\boldsymbol{\psi}}_m \in \breve{\Upsilon}}\ \sum_{m=1}^{M_T^{RF}}\log_2\left(\left|\mathbf{I}_{M_R} + \frac{p}{M_T^{RF}\sigma^2}\tilde{\boldsymbol{\psi}}_m^H\breve{\mathbf{Q}}_{m-1}\tilde{\boldsymbol{\psi}}_m\right|\right). \tag{20}$$

With this formulation, the singular value decomposition of $\breve{\mathbf{Q}}_{m-1} = \mathbf{U}\Sigma\mathbf{U}^H$ can be used to find the optimal precoder. Particularly, the optimal precoder $\tilde{\boldsymbol{\psi}}_m^{opt}$ can be equal to the right singular vector $\mathbf{u}_1$. However, the key limitation is that it may not satisfy the equal amplitude constraint on $\tilde{\boldsymbol{\psi}}_m^{opt}$. Therefore, the maximization problem can be equivalently written as a minization of the squared error distance $||\mathbf{u}_1 - \boldsymbol{\psi}_m||_2^2$. The modified optimization problem is given as

$$\tilde{\boldsymbol{\psi}}_m^{opt} = \arg\min_{\tilde{\boldsymbol{\psi}}_m \in \breve{\Upsilon}}\ ||\mathbf{u}_1 - \boldsymbol{\psi}_m||_2^2. \tag{21}$$

Finally, the solution to this problem is given as [15]

$$\tilde{\boldsymbol{\psi}}_m^{opt} = \tilde{\psi}_{BB_m}\tilde{\boldsymbol{\psi}}_{RF_m} = \frac{||\mathbf{u}||_1}{M_T^{RF}}. \tag{22}$$

Similarly, optimum precoders for other sub-arrays can be found that can be used in step 6 onwards in Algorithm 1. Note that the complexity of the SIC algorithm can be reduced by utilizing power iteration method [45], with number of iterations set to $\mathcal{K}$.

IV. SIMULATION RESULTS

This section will provide numerical evaluation of the considered joint cBPSO and SIC based antenna selection and precoding scheme. Firstly, the proposed scheme will be compared with the optimal ES and other popular approaches in terms of SE. A comparison with other state of the art meta heuristic algorithm will also be shown. Secondly, a comparison for different number of transmit antenna elements M_T while varying the number selected antennas will be presented. Thirdly, EE improvement of the proposed scheme and its trade-off with SE will be demonstrated. Fourthly, a feasibility of the proposed scheme for different hybrid architectures will be shown, followed by a discussion on SE achieved by the proposed scheme in case of an imperfect CSI. Finally, a discussion on computational complexity and an extension to wideband systems will also be provided.

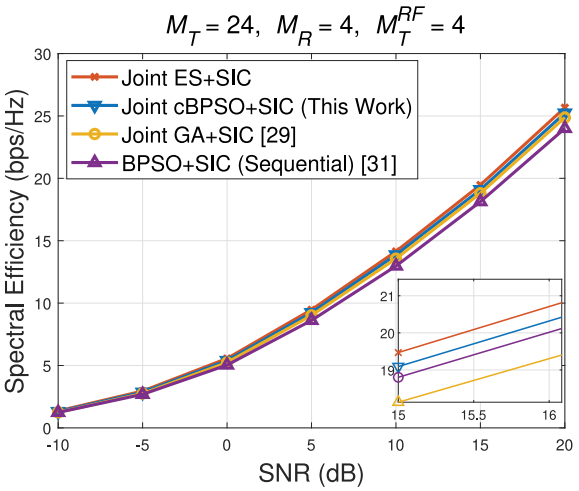

FIGURE 2. Comparison of the proposed scheme with the optimal Exhaustive search and other popular antenna selection. For all plots, precoding is done with SIC algorithm.

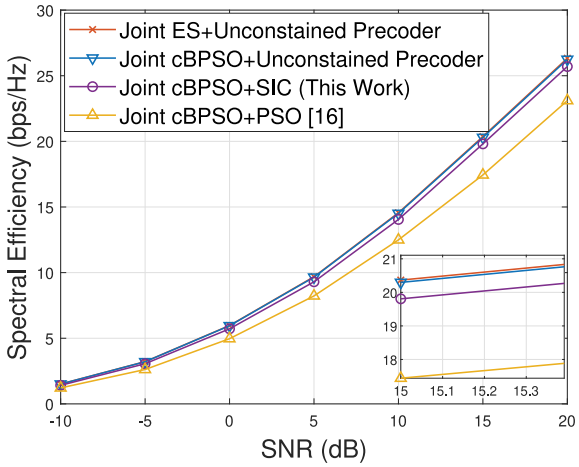

FIGURE 3. Comparison of the proposed scheme with the optimal precoder and a PSO based precoder. For all plots, antenna selection is done with cBPSO algorithm.

A. COMPARISON OF ANTENNA SELECTION SCHEMES

Figure 2 illustrates the comparison of the proposed joint cBPSO+SIC with ES+SIC, GA+SIC and sequential BPSO and SIC. For simulations, M_T is set to 24, $M_T^{RF} = 4$ and $M_R = 4$ while M_T^{Sel} is equal to 4. The schemes are compared in terms of the achieved SE vs SNR. Note that SIC algorithm is used for precoding in all schemes. The results demonstrate that the proposed scheme exhibits performance very similar to that of the ES scheme irrespective of the SNR. This highlights the efficacy of the proposed algorithm. The joint cBPSO+SIC scheme outperforms the GA+SIC scheme with a marginal gap. Finally, BPSO+SIC (sequential) achieves the lowest SE due the sequential nature of the algorithm, i.e., the antenna selection and the precoding are implemented independently. Observe that the difference in the performance of the proposed scheme and BPSO+SIC also increases with SNR. For instance, the SE difference between the schemes at SNR $= 0$ dB and $= 10$ dB is 0.5 and 0.93 bps/Hz, respectively.

B. COMPARISON OF PRECODING SCHEMES

Figure 3 shows the comparison of different precoding schemes, with the common inclusion of cBPSO based antenna selection in all considered scenarios. For simulations, $M_T = 24$ and $M_{Sel} = 16$. The performance of the proposed joint cBPSO+SIC is compared with the PSO and unconstrained precoding [15], i.e., there is no constant amplitude constraint on the amplitude of the analog precoder. Note that unconstrained precoding with ES based antenna selection provides the optimal solution. It can be observed that the performance of joint cBPSO+SIC is very close to the ES+Unconstrained (optimal) precoder. Particularly, the difference between the optimal and SIC based precoder at SNR $= 5$ dB is 0.386 bits/s/Hz. Furthermore, due to relatively high ratio of selected antennas compared to the total number of available antennas, the optimal cBPSO+Unconstrained precoder performs very close to the ES+Unconstrained precoder. Finally, PSO based precoder achieves the lowest SE and the difference with the optimal scheme at SNR $= 5$ dB is 1.46 bits/s/Hz.

C. EFFECT OF AN INCREASE IN M_{SEL}

The comparison in the SE with different M_{Sel} is shown in Figure 4. The total number of transmit antenna are set to $M_T = 256$ while $M_T^{RF} = 4$ and $M_R = 4$. The number of selected antennas are varied as $M_{Sel} = 64, 128, 192$. A significant improvement in the SE can be observed when M_{Sel} is increased from 64 to 128. However, the performance decreases with a further increase in M_{Sel}. Particularly, at SNR $= 10$ dB, the achieved SE is 18.43, 21.34, 22.92 and 23.56 bps/Hz for $M_{Sel} = 64, 128, 192$ and full array, i.e., $M_T = 256$, respectively. Note that the difference in the SE achieved by the full array with $M_{Sel} = 64$ is very large 5.13 bps/Hz whereas with $M_{Sel} = 192$ the difference reduces to only 0.64 bps/Hz. This signifies that the selection of the appropriate number antennas can achieve a similar SE as compared to a full array.

D. POWER CONSUMPTION AND EE

It has been seen that the considered antenna selection scheme can attain a SE similar to that of a full array. The next important metric is to compare the power consumption with different M_{Sel} and the full array. The total power consumption P_{Tot} is computed as

$$P_{Tot} = P_t + M_T^{RF} P_{RF} + M_{Sel} P_{PS} + M_T P_S, \tag{23}$$

where P_t represents the transmitted power, P_{RF}, P_{PS} and P_S are the power consumed by the radio frequency chain, phase shifter and switch, respectively. In this work, $P_t = 1$ W, $P_{RF} = 250$ mW [46] and $P_{PS} = 30$ mW [47]. Note that a switch is connected to each antenna chain to perform antenna selection. Silicon-germanium switches are shown to consume less power while achieving the high performance.

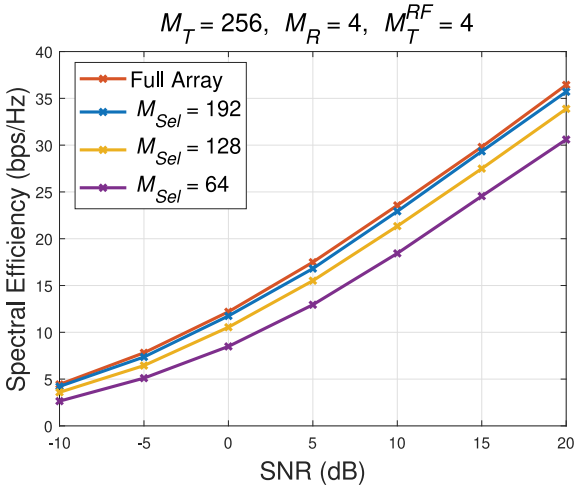

FIGURE 4. Comparison of the proposed scheme for different number of selected antennas. The performance between the full array and the antenna selected scheme decreases with an increase in M_{Sel}.

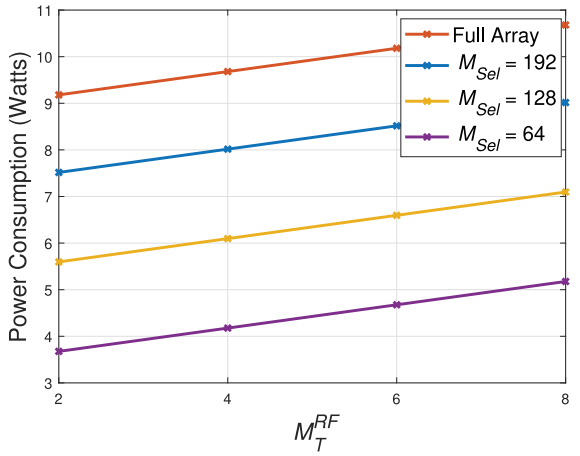

FIGURE 5. Power consumption comparison for different number of selected antennas with a full array.

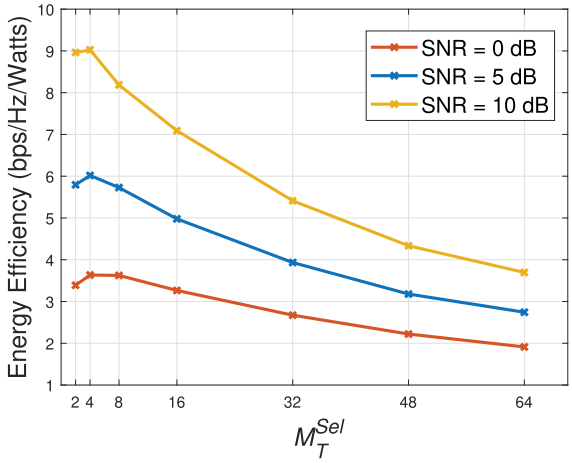

FIGURE 6. EE comparison for different number of selected antennas with a full array.

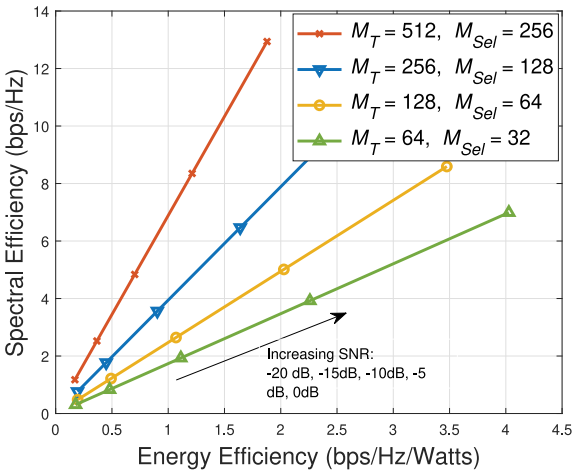

FIGURE 7. EE and SE trade-off with respect to SNR, number of selected antennas and total number of antennas.

In this work, the power consumption a switch is set to $P_S = 1$ mW [48].

The result for a power consumption vs M_T^{RF} comparison for a different number of M_{Sel} and a full array is shown in Figure 5. It is evident from the results that the power consumption increases with M_{Sel}. Note that the switches are not part of a full array system and it consumes a high power irrespective of M_T^{RF}.

Figure 6 shows an EE based comparison of the antenna selection scheme with the full array. Horizontal axis corresponds to the number of selected antennas per sub-array, and therefore, $M_T^{Sel} = 64$ corresponds to a full array with $M_T = 256$ antennas. The full array system performs worst in terms of EE for SNR $= 0,\ 5$, and 10 dB. Furthermore, there exists an optimal value of M_{Sel} that maximizes the EE. As shown in the figure that for SNR $= 5$ and 10 dB, $M_T^{Sel} = 4$ achieves the maximum EE whereas for SNR $= 0$ dB the optimal number is $M_T^{Sel} = 8$. Note that the maximum EE decreased with a decrease in the SNR. This is because the power consumption is independent of the SNR whereas spectral decreases with the SNR. Finally, the gap between the maximum EE and the EE attained with the full array increases with the SNR. For instance, at SNR $= 0$ dB, the difference between the maximum EE and the full array is 0.91 bps/Hz/Watts whereas for SNR $= 10$ dB the difference increases to 2.81 bps/Hz/Watts.

E. EE VS SE TRADE-OFF

As highlighted in previous subsections, SE increases with M_T, however, EE starts to decrease after a certain increase in M_T. Figure 7 provides further details in this aspect by comparing the EE and SE in different SNR regimes. For each line the SNR increases from $-20, -15, -10, -5$ and 0 dB. Particularly, the left most and right most points correspond to SNR $= -20$ and 0 dB, respectively. The number of transmit antennas are set to 64, 128, 256 and 512, whereas in each case 50% of the antennas are selected. The number of RF chains $M_T^{RF} = 4$ and $M_R = 4$. From this figure,

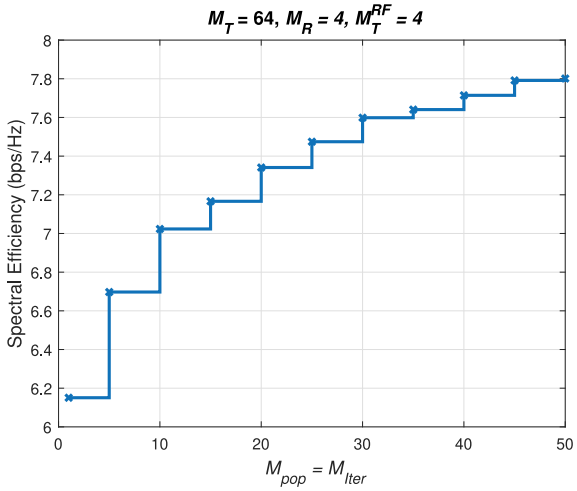

FIGURE 8. Effect of M_{pop} and M_{Iter} on BPSO performance. In this plot $M_{pop} = M_{Iter}$.

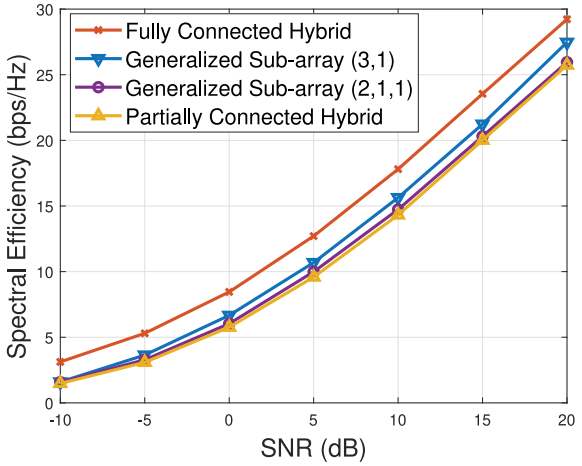

FIGURE 9. Comparison of different hybrid architecture while performing joint antenna selection and precoding. For simulations, $M_T = 64$, $M_{Sel} = 16$ and $M_T^{RF} = 4$. For all architectures, antenna selection is performed using cBPSO algorithm.

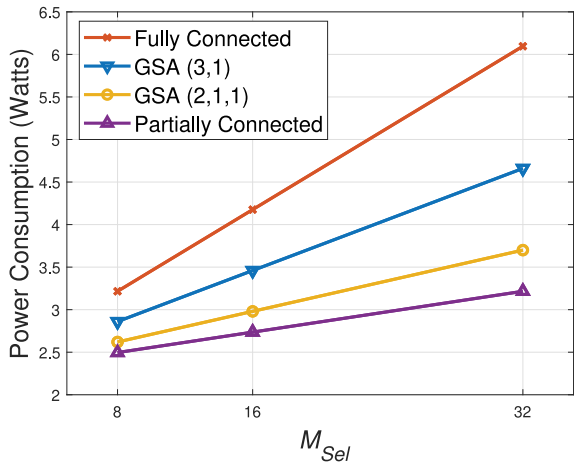

FIGURE 10. Power consumption comparison of a fully connected, a partially connected and a generalized sub-array connected hybrid architectures.

it is evident that both the SE and EE increase with the SNR for all considered values for M_T. This is because that a higher SNR results in an increase in SE whereas the power consumption remains unchanged, and therefore, EE also increases. Furthermore, a higher M_T corresponds to a higher SE irrespective of the SNR. On the other hand, the EE trend for different M_T changes with the SNR. Particularly, at a lower SNR $= -20$ dB, $M_T = 64$ achieves the least EE $= 0.1017$ bps/Hz/Watts whereas $M_T = 256$ scenario achieves the highest EE $= 0.1254$ bps/Hz/Watts and a further increase in M_T decreases the EE. This is due to fact that an initial increase in M_T increase the SE at higher rate compared to an increase in the power consumption, which results in an increase in the EE. However, when antennas are increased from $M_T = 256$ to $M_T = 512$, the power consumption increases faster than SE and thus result in a decrease in EE. Finally, with an increase in SNR, the maximum value of EE starts to shift towards lower M_T. Particularly, from SNR -5 dB onwards, $M_T = 64$ achieves the highest EE. This is because at a higher SNR, the rate at which SE increases with M_T is lower than the corresponding increase in power consumption and thus EE decreases with an increase in M_T.

F. CONVERGENCE OF BPSO ALGORITHM

As discussed earlier that the performance of BPSO algorithm is governed by M_{pop} and M_{Iter}. These are the two tuneable parameters of the BPSO algorithm. If the population size or iterations are increased, BPSO will produce a better result, but the computing complexity will also rise. Figure 8 demonstrates the effects of variable number of iteration and number of agents on the convergence of cBPSO algorithm. SE is plotted for various values of M_{pop} and M_{Iter}, and it is considered that $M_{pop} = M_{Iter}$. As evident from the plot that an initial increase in M_{pop} and M_{Iter} present a considerable increase in SE. However, improvement in the SE decreases with a further increase in M_{pop} and M_{Iter}. Particularly, after $M_{pop} = M_{Iter} = 30$, there is no notable improvement in SE whereas the increase in the computational complexity will be substantial and thus not suitable from implementation perspective.

G. COMPARISON OF DIFFERENT HYBRID ARCHITECTURES

Numerous hybrid architectures have been suggested in the literature for mm-Wave systems. A comparison between three architectures: fully-connected [13], a partially connected [15] and a generalized sub-array (GSA) connected [49] hybrid architectures has been carried out. For simulations, $M_T = 64$, $M_{Sel} = 16$ and $M_T^{RF} = 4$. For GSA, two options, i.e., $(3, 1)$ and $(2, 1, 1)$ have been considered, where $(3, 1)$ means 3 RF chains are connected to a single sub-array whereas 1 is connected to a different sub-array as mentioned in [49].

Figures 9 and 10 compare different hybrid architectures in terms of SE and power consumption, respectively. From Figure 9, it can be observed that a fully-connected architecture achieves a highest SE followed by the GSA-architecture.

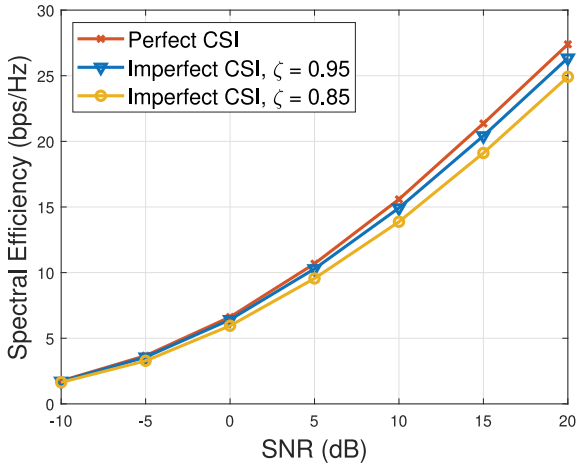

FIGURE 11. Effect of Imperfect CSI on the SE performance.

Note that the achievable SE of GSA-architecture varies based on the number of RF chains that are connected to a particular sub-array. Finally, partially-connected architecture achieves the lowest SE as compared to fully-connected and GSA-connected architecture. From Figure 10 it can be observed that the power consumption comparison follows an opposite trend, i.e., a partially-connected architecture consumes lowest whereas a fully-connected architecture consumes highest power. Power consumption of GSA $(2, 1, 1) < (3, 1)$ configuration. When contemplating future net-zero-aware wireless communication systems, it is essential to recognize that a GSA-connected architecture provides more flexibility. With GSA-connected architecture, we can adjust both the SE and power consumption of the system as compared to the fully- or partially-connected architectures.

H. EFFECT OF IMPERFECT CSI

Acquiring perfect CSI under practical conditions is challenging. To address this, the performance of the proposed scheme is now evaluated in case of an imperfect CSI. With $\mathbf{G}$ representing the channel corresponding to a perfect CSI, the estimated channel incase of an imperfect CSI is given as [15]

$$\hat{\mathbf{G}} = \zeta \mathbf{G} + \sqrt{1-\zeta^2}\mathbf{E}, \tag{24}$$

where $\zeta \in [0, 1]$ represents the precision of the CSI and $\mathbf{E}$ is a $\mathcal{CN}(0, 1)$ independent and identically distributed error matrix. A comparison result of perfect CSI scenario with an imperfect one is shown in Figure 11. The performance is compared in terms of SNR vs SE for $\zeta = 1$, i.e., perfect CSI and $\zeta = 0.95$ and 0.85 for an imperfect CSI scenario. It can be seen that the performance only marginally degrades in case of unavailability of the perfect CSI. This indicates that the system maintains its effectiveness and reliability, despite uncertainties in the CSI, making it a viable solution for real-world practical implementations.

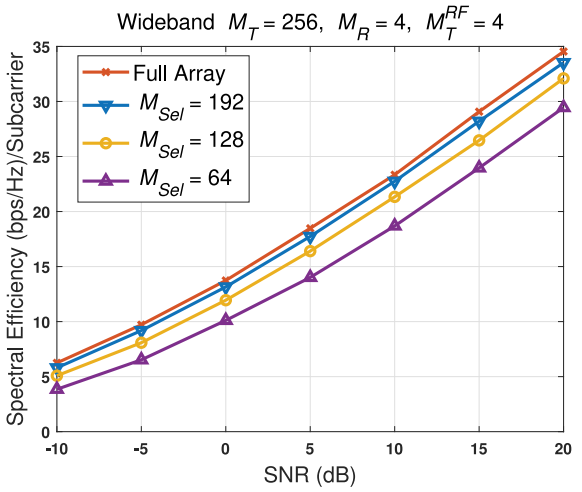

FIGURE 12. Comparison of the proposed scheme for different number of selected antennas in case of a wideband system. The performance between the full array and the antenna selected scheme decreases with an increase in M_{Sel}.

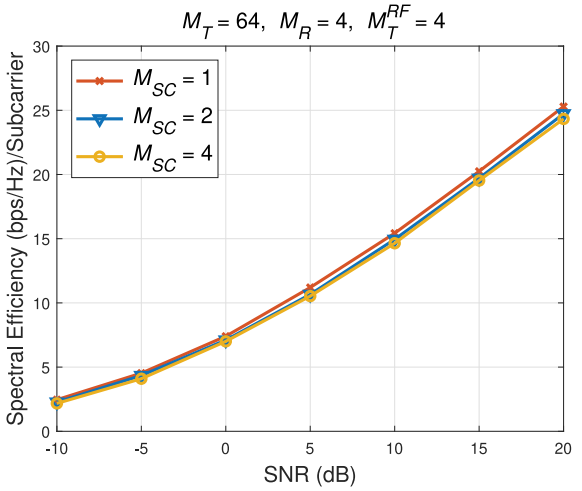

FIGURE 13. Spectral efficiency for different number of sub-carriers M_{SC} with $M_{Sel} = 16$.

I. EXTENSION TO A WIDEBAND SYSTEM

Wideband systems are an integral part of current 5G and future 6G wireless networks. There have been notable efforts from the research community to investigate these systems with a particular effort on devising efficient precoding schemes [50], [51], [52]. Figure 12 and 13 show the effect of M_{Sel} and the number of sub-carriers M_{SC}, respectively, for a wideband system.

From Figure 12, it can be observed that the SE/subcarrier improves by increasing the M_{Sel}. One can notice a consistent increase of 2 to 3 dB in gain across the SNR range from -10 till 20 dB as the value of M_{Sel} rises from 64 to 128. Further improvement can be observed when M_{Sel} is increased to 192 where the performance is less than a dB away from the fully-connected structure. Similar to the narrowband case (see Figure 4) the improvement in SE increases with an increase in M_{Sel}. This validates that the proposed solution can be easily scale able to wideband systems.

Finally, Figure 13 compares the SE/subcarrier for different values of M_{SC}. It can be observed that the performance of $M_{SC} = 1, 2$ and 4 is very similar. For instance, at SNR $= 0$ dB, the achievable SE/subcarrier is 7.4, 7.1, 7 for $M_{SC} = 1, 2$ and 4, respectively. Therefore, it is evident that the proposed scheme can work for both the narrowband and wideband systems.

J. COMPLEXITY ANALYSIS

For the analysis of computational complexity, we have to take into account the number of complex additions and complex multiplications required for selection algorithms (cBPSO, GA and Exhaustive) and precoding algorithms (SIC and PSO).

GA and cBPSO requires $N_{pop} \times N_{iter} \times \Delta$ (where Δ represent the complexity of the fitness function) complex operations of multiplications and additions [31]. Note that both GA and cBPSO has a similar complexity. However, cBPSO achieves a higher SE, and therefore, also result in a higher EE. On the other hand, the exhaustive search algorithm requires to evaluate $\mathcal{S}_t = (\mathcal{S}_c)^{M_T^{RF}}$, where $\mathcal{S}_c = \binom{M_{Sub}}{M_T^{Sel}}$, combinations to find the optimal solution. Even in a straightforward scenario with $M_{Sub} = 16$, $M_T^{RF} = 4$ and $M_T^{Sel} = 4$, this leads to a total of 1×10^{13} combinations. Therefore, the increased complexity of an exhaustive search algorithm, especially with a comparable size of the antenna array, renders it impractical for implementation in massive MIMO systems.

Note that in simultaneous antenna selection and precoding, the precoding algorithm is implemented during each iteration of the selection algorithm. The computational complexity of SIC based precoding scheme is calculated to be $O(2M_T^{RF}\mathcal{K}((M_T^{Sel})^2(M_R + \mathcal{K}M_T^{RF})))$ as mentioned in [15]. Furthermore, the computational complexity of PSO based precoding is $O(N_{pop}N_{iter}M_R{M_{Sel}}^2)$. Note that N_{pop} and N_{iter} should be increased to improve the SE performance of PSO. Nevertheless, such arrangement leads to a significant increase in the computational complexity of the algorithm.

Finally, the GSA-connected hybrid architecture, that allows a variable number of RF chains connected to sub arrays, incorporates the SIC algorithm. It is important to note that the number of RF chains connected to a sub-array and the number of antennas in each sub-array can be adjusted or varied. Therefore, the complexity of SIC algorithm for GSA is higher compared to SIC applied to a partially connected architecture. In GSA architecture, the number of RF chains required to be connected to each sub array is determined through exhaustive search, leading to an increased computational complexity.

V. CONCLUSION

Focusing on the reduction in the power consumption and enhancing the EE without any notable reduction in SE for future large antenna system, this work proposed a joint antenna selection and precoding scheme. Particularly, a meta-heuristic algorithm cBPSO was devised for an antenna selection while precoding is performed using successive interference cancellation. Results showed that the proposed algorithm achieved a SE close to an optimal ES based antenna selection. Furthermore, it was presented that the proposed scheme improves the EE. It was shown that there is an optimal number of selected antennas that maximize EE. A trade-off between SE and EE was also conducted.

REFERENCES

[1] "What is climate change?" Accessed: Aug. 11, 2023. [Online]. Available: https://climate.nasa.gov/

[2] J. Tollefson, "How hot will Earth get by 2100," *Nature*, vol. 580, no. 7804, pp. 443–445, 2020.

[3] W. B. Abbas, Q. Z. Ahmed, F. A. Khan, N. S. Mian, P. I. Lazaridis, and P. Sureephong, "Designing future wireless networks (FWN)s with net zero (NZ) and zero touch (ZT) perspective," *IEEE Access*, vol. 11, pp. 83301–83321, 2023.

[4] A. S. G. Andrae and T. Edler, "On global electricity usage of communication technology: Trends to 2030," *Challenges*, vol. 6, no. 1, pp. 117–157, 2015.

[5] S. Han, T. Xie, and C.-L. I, "Greener physical layer technologies for 6G mobile communications," *IEEE Commun. Mag.*, vol. 59, no. 4, pp. 68–74, Apr. 2021.

[6] M. Z. Chowdhury, M. Shahjalal, S. Ahmed, and Y. M. Jang, "6G wireless communication systems: Applications, requirements, technologies, challenges, and research directions," *IEEE Open J. Commun. Soc.*, vol. 1, pp. 957–975, 2020.

[7] S. Sun, T. S. Rappaport, R. W. Heath, A. Nix, and S. Rangan, "MIMO for millimeter-wave wireless communications: Beamforming, spatial multiplexing, or both?" *IEEE Commun. Mag.*, vol. 52, no. 12, pp. 110–121, Dec. 2014.

[8] B. Ning et al., "Beamforming technologies for ultra-massive MIMO in terahertz communications," *IEEE Open J. Commun. Soc.*, vol. 4, pp. 614–658, 2023.

[9] J. Zhang, X. Yu, and K. B. Letaief, "Hybrid beamforming for 5G and beyond millimeter-wave systems: A holistic view," *IEEE Open J. Commun. Soc.*, vol. 1, pp. 77–91, 2020.

[10] C. K. Sheemar, C. K. Thomas, and D. Slock, "Practical hybrid beamforming for millimeter wave massive MIMO full duplex with limited dynamic range," *IEEE Open J. Commun. Soc.*, vol. 3, pp. 127–143, 2022.

[11] W. B. Abbas, F. Gomez-Cuba, and M. Zorzi, "Millimeter wave receiver efficiency: A comprehensive comparison of beamforming schemes with low resolution ADCs," *IEEE Trans. Wireless Commun.*, vol. 16, no. 12, pp. 8131–8146, Dec. 2017.

[12] O. Alluhaibi, Q. Z. Ahmed, E. Kampert, M. D. Higgins, and J. Wang, "Revisiting the energy-efficient hybrid D-A precoding and combining design for mm-wave systems," *IEEE Trans. Green Commun. Netw.*, vol. 4, no. 2, pp. 340–354, Jun. 2020.

[13] O. E. Ayach, S. Rajagopal, S. Abu-Surra, Z. Pi, and R. W. Heath, "Spatially sparse precoding in millimeter wave MIMO systems," *IEEE Trans. Wireless Commun.*, vol. 13, no. 3, pp. 1499–1513, Mar. 2014.

[14] X. Yu, J.-C. Shen, J. Zhang, and K. B. Letaief, "Alternating minimization algorithms for hybrid precoding in millimeter wave MIMO systems," *J. Sel. Topics Signal Process.*, vol. 10, no. 3, pp. 485–500, Apr. 2016.

[15] X. Gao, L. Dai, S. Han, C.-L. I, and R. W. Heath, "Energy-efficient hybrid analog and digital precoding for mmWave MIMO systems with large antenna arrays," *IEEE J. Sel. Areas Commun.*, vol. 34, no. 4, pp. 998–1009, Apr. 2016.

[16] O. Alluhaibi, Q. Z. Ahmed, J. Wang, and H. Zhu, "Hybrid digital-to-analog precoding design for mm-wave systems," in *Proc. IEEE Int. Conf. Commun. (ICC)*, Paris, France, 2017, pp. 1–6.

[17] S. Khalid, W. B. Abbas, H.S. Kim, and M. T. Niaz, "Evolutionary algorithm based capacity maximization of 5G/B5G hybrid pre-coding systems," *Sensors*, vol. 20, no. 18, p. 5338, 2020.

[18] T. Shen, Y. Lin, J. Zou, Y. Wu, F. Shu, and J. Wang, "Low-complexity leakage-based secure precise wireless transmission with hybrid beamforming," *IEEE Wireless Commun. Lett.*, vol. 9, no. 10, pp. 1687–1691, Oct. 2020.

[19] K. Ardah, G. Fodor, Y. C. B. Silva, W. C. Freitas, and F. R. P. Cavalcanti, "A unifying design of hybrid beamforming architectures employing phase shifters or switches," *IEEE Trans. Veh. Technol.*, vol. 67, no. 11, pp. 11243–11247, Nov. 2018.

[20] K. Ardah, G. Fodor, Y. C. B. Silva, W. C. Freitas, and A. L. F. de Almeida, "Hybrid analog-digital beamforming design for SE and EE maximization in massive MIMO networks," *IEEE Trans. Veh. Technol.*, vol. 69, no. 1, pp. 377–389, Jan. 2020.

[21] D. Zhang, Y. Wang, X. Li, and W. Xiang, "Hybridly connected structure for hybrid beamforming in mmWave massive MIMO systems," *IEEE Trans. Commun.*, vol. 66, no. 2, pp. 662–674, Feb. 2018.

[22] X. Liu et al., "Hybrid precoding for massive mmWave MIMO systems," *IEEE Access*, vol. 7, pp. 33577–33586, 2019.

[23] J. S. Thompson et al., "Editorial a decade of green radio and the path to "net zero": A United Kingdom perspective," *IEEE Trans. Green Commun. Netw.*, vol. 6, no. 2, pp. 657–664, Jun. 2022.

[24] A. F. Molisch, M. Z. Win, Y.-S. Choi, and J. H. Winters, "Capacity of MIMO systems with antenna selection," *IEEE Trans. Wireless Commun.*, vol. 4, no. 4, pp. 1759–1772, Jul. 2005.

[25] S. Asaad, A. M. Rabiei, and R. R. Müller, "Massive MIMO with antenna selection: Fundamental limits and applications," *IEEE Trans. Wireless Commun.*, vol. 17, no. 12, pp. 8502–8516, Dec. 2018.

[26] Y. Zhang, G. Zheng, C. Ji, K.-K. Wong, D. J. Edwards, and T. Cui, "Near-optimal joint antenna selection for amplify-and-forward relay networks," *IEEE Trans. Wireless Commun.*, vol. 9, no. 8, pp. 2401–2407, Aug. 2010.

[27] R. Rajashekar, L.-L. Yang, K. V. S. Hari, and L. Hanzo, "Transmit antenna subset selection in generalized spatial modulation systems," *IEEE Trans. Veh. Technol.*, vol. 68, no. 2, pp. 1979–1983, Feb. 2019.

[28] B. S. Tan, K. H. Li, and K. C. Teh, "Transmit antenna selection systems: A performance comparison of different types of receiver schemes," *IEEE Veh. Technol. Mag.*, vol. 8, no. 3, pp. 104–112, Sep. 2013.

[29] B. Makki, A. Ide, T. Svensson, T. Eriksson, and M.-S. Alouini, "A genetic algorithm-based antenna selection approach for large-but-finite MIMO networks," *IEEE Trans. Veh. Technol.*, vol. 66, no. 7, pp. 6591–6595, Jul. 2017.

[30] S. Jang, M. Ahn, H. Lee, and I. Lee, "Antenna selection schemes in bidirectional full-duplex MIMO systems," *IEEE Trans. Veh. Technol.*, vol. 65, no. 12, pp. 10097–10100, Dec. 2016.

[31] S. Khalid, R. Mehmood, W. B. Abbas, F. Khalid, and M. Naeem, "Joint transmit antenna selection and precoding for millimeter wave massive MIMO systems," *Phys. Commun.*, vol. 42, Oct. 2020, Art. no. 101137.

[32] F. Ahmad, W. B. Abbas, S. Khalid, F. Khalid, I. Khan, and F. Aldosari, "Performance enhancement of mmWave MIMO systems using machine learning," *IEEE Access*, vol. 10, pp. 73068–73078, 2022.

[33] H. Li, Q. Liu, Z. Wang, and M. Li, "Joint antenna selection and analog precoder design with low-resolution phase shifters," *IEEE Trans. Veh. Technol.*, vol. 68, no. 1, pp. 967–971, Jan. 2019.

[34] X. Zhai, Q. Shi, Y. Cai, and M. Zhao, "Joint transmit precoding and receive antenna selection for uplink multiuser massive MIMO systems," *IEEE Trans. Commun.*, vol. 66, no. 11, pp. 5249–5260, Nov. 2018.

[35] X. Zhai, Y. Cai, Q. Shi, M. Zhao, G. Y. Li, and B. Champagne, "Joint transceiver design with antenna selection for large-scale MU-MIMO mmWave systems," *IEEE J. Sel. Areas Commun.*, vol. 35, no. 9, pp. 2085–2096, Sep. 2017.

[36] V. V. Ratnam, A. F. Molisch, O. Y. Bursalioglu, and H. C. Papadopoulos, "Hybrid beamforming with selection for multiuser massive MIMO systems," *IEEE Trans. Signal Process.*, vol. 66, no. 15, pp. 4105–4120, Aug. 2018.

[37] C. Ouyang, S. Wu, C. Jiang, D. W. K. Ng, and H. Yang, "Receive antenna selection under discrete inputs: Approximation and applications," *IEEE Trans. Commun.*, vol. 68, no. 4, pp. 2634–2647, Apr. 2020.

[38] J. Chen, S. Chen, Y. Qi, and S. Fu, "Intelligent massive MIMO antenna selection using monte carlo tree search," *IEEE Trans. Signal Process.*, vol. 67, no. 20, pp. 5380–5390, Oct. 2019.

[39] M. O. K. Mendonça, P. S. R. Diniz, T. N. Ferreira, and L. Lovisolo, "Antenna selection in massive MIMO based on greedy algorithms," *IEEE Trans. Wireless Commun.*, vol. 19, no. 3, pp. 1868–1881, Mar. 2020.

[40] S. Wang, M. Zhu, Z. Li, L. Yang, C.-X. Wang, and R. Ruby, "Antenna selections strategies for massive MIMO systems with limited-resolution ADCs/DACs," *IEEE Trans. Wireless Commun.*, vol. 22, no. 11, pp. 8128–8140, Nov. 2023.

[41] W. B. Abbas, F. Gomez-Cuba, and M. Zorzi, "Bit allocation for increased power efficiency in 5G receivers with variable-resolution ADCs," in *Proc. Inf. Theory Appl. Workshop (ITA)*, San Diego, CA, USA, 2017, pp. 1–7.

[42] M. Nair, Q. Z. Ahmed, and H. Zhu, "Hybrid digital-to-analog beamforming for millimeter-wave systems with high user density," in *Proc. IEEE Glob. Commun. Conf. (GLOBECOM)*, Washington, DC, USA, 2016, pp. 1–6.

[43] Q. Z. Ahmed, S. Ahmed, M.-S. Alouini, and S. Aïssa, "Minimizing the symbol-error-rate for amplify-and-forward relaying systems using evolutionary algorithms," *IEEE Trans. Commun.*, vol. 63, no. 2, pp. 390–400, Feb. 2015.

[44] S. Mirjalili and A. Lewis, "S-shaped versus V-shaped transfer functions for binary particle swarm optimization," *Swarm Evolut. Comput.*, vol. 9, pp. 1–14, Apr. 2013.

[45] G. H. Golub and C. F. Van Loan, *Matrix Computations*. Baltimore, MD, USA: JHU Press, 2012.

[46] P. V. Amadori and C. Masouros, "Low RF-complexity millimeter-wave beamspace-MIMO systems by beam selection," *IEEE Trans. Commun.*, vol. 63, no. 6, pp. 2212–2223, Jun. 2015.

[47] R. Méndez-Rial, C. Rusu, N. González-Prelcic, A. Alkhateeb, and R. W. Heath, "Hybrid MIMO architectures for millimeter wave communications: Phase shifters or switches?" *IEEE Access*, vol. 4, pp. 247–267, 2016.

[48] A. Haqiqatnejad, F. Kayhan, and B. Ottersten, "Energy-efficient hybrid symbol-level precoding for large-scale mmWave multiuser MIMO systems," *IEEE Trans. Commun.*, vol. 69, no. 5, pp. 3119–3134, May 2021.

[49] Y. Chen, D. Chen, T. Jiang, and L. Hanzo, "Millimeter-wave massive MIMO systems relying on generalized sub-array-connected hybrid precoding," *IEEE Trans. Veh. Technol.*, vol. 68, no. 9, pp. 8940–8950, Sep. 2019.

[50] Y. Chen, D. Chen, T. Jiang, and L. Hanzo, "Channel-covariance and angle-of-departure aided hybrid precoding for wideband multiuser millimeter wave MIMO systems," *IEEE Trans. Commun.*, vol. 67, no. 12, pp. 8315–8328, Dec. 2019.

[51] Y. Chen, Y. Xiong, D. Chen, T. Jiang, S. X. Ng, and L. Hanzo, "Hybrid precoding for wideband millimeter wave MIMO systems in the face of beam squint," *IEEE Trans. Wireless Commun.*, vol. 20, no. 3, pp. 1847–1860, Mar. 2021.

[52] L. Dai, J. Tan, Z. Chen, and H. V. Poor, "Delay-phase precoding for wideband THz massive MIMO," *IEEE Trans. Wireless Commun.*, vol. 21, no. 9, pp. 7271–7286, Sep. 2022.

WAQAS BIN ABBAS received the bachelor's and master's degrees from the National University of Computer and Emerging Sciences, Islamabad, Pakistan, in 2008 and 2012, respectively, and the Ph.D. degree in information engineering from the University of Padova, Italy, in 2017. He was a Postdoctoral Research Fellow with the University of Huddersfield, U.K., from February 2022 till December 2022. He is currently working as a Lecturer with the School of Electrical, Electronic and Mechanical Engineering, University of Bristol, U.K. During master's, his research was focused in underwater wireless communication, while during Ph.D., his research was mostly focused on energy efficiency in wireless networks. His current research interests include energy efficiency in 5G and beyond cellular networks, MIMO communication, and multi-hop wireless networks.

SALMAN KHALID received the bachelor's degree from the University of Engineering and Technology, Taxila, Pakistan, in 2008, the master's degree from the Center of Advanced Studies in Engineering, Islamabad, Pakistan, in 2014, and the Ph.D. degree in electrical engineering from the National University of Computer and Emerging Sciences, Islamabad, in 2022. During master's degree, his research was focused on wireless communication, compressed sensing and digital signal processing, while during Ph.D. degree, his research was mostly focused on hybrid precoder design, resource allocation in MIMO communication networks and energy efficiency in wireless networks. His current research interests include energy efficiency in 5G/6G millimeter-wave cellular networks, MIMO communication, and millimeter-wave hybrid beamforming.

QASIM ZEESHAN AHMED (Member, IEEE) received the Ph.D. degree from the University of Southampton, Southampton, U.K., in 2009. He worked as an Assistant Professor with the National University of Computer and Emerging Sciences (NUCES-FAST), Islamabad, Pakistan, from November 2009 to June 2011. He was a Postdoctoral Fellow with the Computer, Electrical and Mathematical Sciences and Engineering Division, King Abdullah University of Science and Technology, Thuwal, Saudi Arabia, from June 2011 to June 2014. He joined the University of Kent, U.K., as a Lecturer from January 2015 to January 2017. He was a Lecturer, then a Senior Lecturer, and currently a Reader of Electronic Engineering with the School of Computing and Engineering, University of Huddersfield, U.K., in 2017, 2018, and 2020, respectively. He is currently a Principal Investigator, U.K. for Erasmus + DigiHealth-Asia Project and the MSCA Staff Exchanges EVOLVE Project. He is a Co-Investigator of EU H2020 ETN Research MOTOR5G Project and EU H2020 RISE Research RECOMBINE Project. His research interests include mainly ultrawide bandwidth systems, millimeter waves, device to device, digital health, and cooperative communications. He is a Fellow of Higher Education Academy.

FARHAN KHALID (Member, IEEE) received the B.S. degree in electronic engineering from the Ghulam Ishaq Khan Institute of Engineering Sciences Technology, Topi, Pakistan, in 1999, the master's degree in telecommunication management from the Institut National des Telecommunications, France, in 2001, the M.Sc. degree in electrical engineering from the Blekinge Institute of Technology, Karlskrona, Sweden, in 2005, and the Dr.-Ing. (Ph.D.) degree in electrical engineering from the University of Stuttgart, Stuttgart, Germany, in 2012. He started his professional career as an engineer, working for various organizations in the telecom sector. Since 2006, he has been involved with academia and research in the domains of digital communications and signal processing and is currently associated with the Department of Electrical Engineering, National University of Computer and Emerging Sciences, Islamabad, Pakistan. His current research interests lie in the area of wireless communications, with particular focus on transceiver design and optimization for multiuser massive MIMO and millimeter wave systems.

TEMITOPE T. ALADE received the B.Sc. degree in computer science from the University of Ilorin in 2003, the M.Sc. degree in mobile computing from the University of Bradford in 2007, and the Ph.D. degree in electronic engineering from the University of Kent in 2012. He is currently an Associate Professor of Computing Sciences with the School of Computing Sciences, University of East Anglia. From June 2020 to December 2022, he was a Senior Lecturer of Computer Science with Nottingham Trent University, where he was the Course Leader for M.Sc. Computer Science, and the M.Sc. Research Project Coordinator. From September 2016 to May 2020, he was a Senior Lecturer of Computing with the Department of Computing, University of Worcester, where he was the Research Excellence Framework Coordinator and a Research Group Coordinator for the Applied Computing Research Group. From September 2015 to August 2016, he was a Teaching Fellow of Computing with the School of Computing and Mathematics, University of Keele. From June 2012 to September 2015, he worked as a Postdoctoral Research Associate and then as a Lecturer of Mobile Communication with the University of Kent. His research interests include modeling and analysis of computing and communication systems, such as those found in mobile communication systems, mobile computing systems, Web-based systems, Internet of Things, machine learning and their applications in every area of public life including, finance, healthcare, wireless networks, buildings, entertainment, and related industries. His research spans the whole spectrum from technical design, through algorithms to system development and performance evaluation.

PRADORN SUREEPHONG was born on 1 April 1980, in Chiang Mai, Thailand. He received the Bachelor of Engineering degree in computer engineering and the Master of Economics degree from Chiang Mai University, and the Doctor of Philosophy degree in cotutelle in Informatics (Informatique) from University Lumiere Lyon2 and in Knowledge Management from Chiang Mai University, where he currently serves as the Head of the Master of Science in Digital Technology Management Program with the College of Arts, Media, and Technology. His research interests include digital transformation for industries, smart city technology, smart agriculture technology, blockchain technology for education, and assistive technology for the wellness industry.